AGU PUBLICATIONS

Geophysical Research Letters

RESEARCH LETTER

10.1002/2014GL060990

Key Points:
- Application of mass loading in the SWMF SC component for sungrazing comets
- Extension to a tail source model for mass loading due to a sungrazing comet
- Prediction of mass-loaded solar wind parameters along a space probe path

Correspondence to:
A. P. Rasca,
rasca@colorado.edu

Citation:
Rasca, A. P., R. Oran, and M. Horányi (2014), Mass loading of the solar wind by a sungrazing comet, *Geophys. Res. Lett.*, *41*, 5376–5381, doi:10.1002/2014GL060990.

Received 23 JUN 2014
Accepted 24 JUL 2014
Accepted article online 28 JUL 2014
Published online 6 AUG 2014

Mass loading of the solar wind by a sungrazing comet

A. P. Rasca[1], R. Oran[2], and M. Horányi[3]

[1]Laboratory for Atmospheric and Space Physics, University of Colorado Boulder, Boulder, Colorado, USA, [2]Department of Atmospheric, Oceanic and Space Sciences, University of Michigan, Ann Arbor, Michigan, USA, [3]Department of Physics, University of Colorado Boulder, Boulder, Colorado, USA

Abstract Collisionless mass loading was suggested by Biermann et al. (1967) for describing interactions between the solar wind and cometary atmospheres. Recent observations have led to an increased interest in coronal mass loading due to sungrazing comets and collisional debris of sunward migrating interplanetary dust particles. In a previous paper, we presented a 3-D MHD model of the solar corona based on the Block-Adaptive-Tree-Solarwind-Roe-Upwind-Scheme code which includes the interaction of dust with the solar wind. We have shown the impact on the solar wind from abrupt mass loading in the coronal region. We apply the model to a sungrazing cometary source, using ejected dust dynamics to generate tail-shaped mass-loading regions. Results help predict the effects on the solar wind acceleration and composition due to sungrazing comets, such as Comet C/2011 W3 (Lovejoy). We show how these effects may be detected by the upcoming Solar Probe Plus Mission.

1. Introduction

The future Solar Probe Plus mission through the solar corona will provide scientists with the first ever in situ measurements of the coronal plasma environment and magnetic field structure. Among the mission objectives is the exploration of the plasma environment near the Sun [*Solar Probe Plus*, 2008]. The plasma environment of the corona is expected to be contaminated by the delivery and collisional breakup of interplanetary dust particles near the Sun [*Mann and MacQueen*, 1996].

Another mechanism for depositing dust particles in the solar corona is via larger objects passing near the Sun, where dust release by sputtering or evaporation may occur. Sungrazing comets provide a common means for dust particle release and pick up by the solar wind, since such comets lose a significant amount of mass (if not all) during their perihelion passage. For example, on 15 December 2011 Comet C/2011 W3 (Lovejoy) saw a significant mass reduction after passing at a height of 0.2 $R_{\odot}$ above the solar surface, leading to a cataclysmic fragmentation [*Sekanina and Chodas*, 2012].

Certain interplanetary magnetic field enhancements have been proposed to result from solar wind interactions with cometary tails or other dust sources [*Russell*, 1990; *Russell et al.*, 2009]. However, with no in situ observations yet for the solar corona, it is uncertain how solar wind parameters near the Sun will be affected by mass loading of these particles.

Recent modeling of mass loading in the solar corona due to dust [*Rasca and Horányi*, 2013; *Rasca et al.*, 2014] included an additional mass-loading feature to a Solar Corona (SC) component of the Space Weather Modeling Framework (SWMF), which uses the Block-Adaptive-Tree-Solarwind-Roe-Upwind-Scheme (BATS-R-US) magnetohydrodynamic (MHD) code. Both BATS-R-US and the SWMF are described in *Tóth et al.* [2012, and references therein]. The MHD + dust coronal model presented by *Rasca et al.* [2014] is an extension of the MHD coronal model described by *van der Holst et al.* [2010].

Rasca et al. [2014] primarily focused on introducing a mass-loading mechanism into the SC model and demonstrating how the solar wind reacts to general mass-loading regions being placed in the subsonic and supersonic wind regions (Figure 5 in their study). Their study introduced a potential sungrazing comet application for the model, where a cometary mass-loading point source is represented by depositing mass-loading particles into a single computational cell at a steady rate. We will expand on this sungrazing comet application by replacing the point source model with a more realistic extended tail source model.

In the next section we provide a brief review of the MHD code and cometary dust mass loss model used by *Rasca et al.* [2014], followed by a description of our cometary tail model, defining a mass-loading region.

We show a mass-loaded solar wind during various stages of a sungrazing cometary trajectory. In section 3 we discuss how a mass-loaded solar wind may appear to Solar Probe Plus as it passes downstream of a cometary source. Lastly, we discuss and summarize our findings.

2. Model Description and Results

We use the modified SC component described by *Rasca et al.* [2014, and references therein] for modeling the solar wind out to 24 $R_\odot$. The intrinsic solar magnetic field is described by an ideal dipole tilted 10° with respect to the solar rotation axis. This model solves a coupled set of 3-D MHD equations on an adaptive grid coupled to a wave kinetic equation for low-frequency Alfvén waves, under the Wentzel-Kramers-Brillouin approximation, that accelerates and heats the plasma along open magnetic field lines. Heating is achieved by turbulent Alfvén wave dissipation as described by *Hollweg* [1986] (see *van der Holst et al.* [2010] for more details). The model splits mass conservation into an equation for hydrogen density ρ_{H} and an equation for ionized dust density ρ_{d_i}, where the total mass density is defined as $\rho = \rho_{\mathrm{H}} + \rho_{d_i}$. The set of resulting MHD equations are

$$\frac{\partial \rho_{\mathrm{H}}}{\partial t} + \nabla \cdot \left(\rho_{\mathrm{H}} \mathbf{u}\right) = 0 \tag{1}$$

$$\frac{\partial \rho_{d_i}}{\partial t} + \nabla \cdot \left(\rho_{d_i} \mathbf{u}\right) = S_{\rho_{d_i}} \tag{2}$$

$$\frac{\partial (\rho \mathbf{u})}{\partial t} + \nabla \cdot \left[\rho \mathbf{u}\mathbf{u} + \left(p + p_W + \frac{B^2}{2\mu_0}\right) I - \frac{\mathbf{B}\mathbf{B}}{\mu_0}\right] = \mathbf{S}_{\rho \mathbf{u}} \tag{3}$$

$$\frac{\partial \mathbf{B}}{\partial t} + \nabla \cdot (\mathbf{u}\mathbf{B} - \mathbf{B}\mathbf{u}) = 0 \tag{4}$$

$$\frac{\partial E}{\partial t} + \nabla \cdot \left[\mathbf{u}\left(E + p + p_W + \frac{B^2}{2\mu_0}\right) - \frac{(\mathbf{u} \cdot \mathbf{B})\,\mathbf{B}}{\mu_0} + \left(E_W^+ - E_W^-\right)\mathbf{u}_{\mathrm{A}}\right] = S_E, \tag{5}$$

where $\mathbf{u}$, p, E, and $\mathbf{B}$ are flow velocity, pressure, energy density, and magnetic field, respectively. B, μ_0, and $\mathbf{u}_{\mathrm{A}}$ represent magnetic field strength, permeability of free space, and Alfvén speed, respectively. The wave energy densities of Alfvén waves propagating parallel and antiparallel to $\mathbf{B}$ are denoted by E_W^+ and E_W^-, respectively. The Alfvén wave energy density and pressure are defined as $E_W = E_W^+ + E_W^-$ and $p_W = E_W/2$, where the former is given by the time-dependent solution of

$$\frac{\partial E_W^\pm}{\partial t} + \nabla \cdot \left[E_W^\pm \left(\mathbf{u} \pm \mathbf{u}_{\mathrm{A}}\right)\right] = -p_W^\pm \nabla \cdot \mathbf{u} - Q^\pm \tag{6}$$

and Q is the wave dissipation term [*van der Holst et al.*, 2010].

The nonzero source terms for equations (1)–(5) are defined as

$$S_{\rho_d} = S_{d1} \tag{7}$$

$$\mathbf{S}_{\rho \mathbf{u}} = \mathbf{S}_{d2} - \rho\left[\frac{GM}{r^3}\mathbf{r} + \Omega \times (\Omega \times r) + 2\Omega \times u\right] \tag{8}$$

$$S_E = S_{d3} - \nabla \cdot \mathbf{q} - \rho \mathbf{u} \cdot \left[\frac{GM}{r^3}\mathbf{r} + \Omega \times (\Omega \times r)\right], \tag{9}$$

where G, M, and Ω are the gravitational constant, solar mass, and solar angular velocity, respectively. The parameter $\mathbf{q}$ is the Spitzer thermal heat flux vector applied within 10 $R_\odot$. The flow is considered collisionless outside this radius. The mass-loading source terms $\mathbf{S}_d = \left(S_{d1}, \mathbf{S}_{d2}, S_{d3}\right)^{\mathrm{T}}$ are the same as described by *Rasca et al.* [2014] and derived from earlier works by *Biermann et al.* [1967]. These space- and time-dependent source terms represent the added mass, momentum, and energy that mass-loading particles add to the solar wind flow. In this study, equations (7)–(9) represent the mass source in the solar wind caused by ionized cometary dust. *Rasca et al.* [2014] used a steady mass-loading rate for a single computational cell to

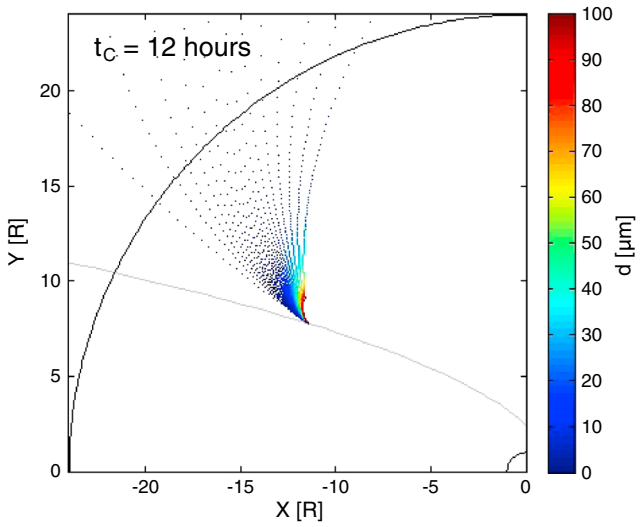

Figure 1. A tail-shaped mass-loading region and particle distributions used to update results for four different times t_C. The example shown is for $t_C = 12$ h. Particles are colored according to diameter d, ranging from 0.1 to 100 μm. The solar surface, cometary orbit, and outer boundary of the SC component domain are drawn.

represent a cometary mass-loading source. Since this model looks at macroscopic changes in the solar wind, we can ignore small-scale instabilities and collisional effects from gyrating pickup ions. Small micron- to submicron-sized particles make up the majority of the mass released and picked up by the solar wind, which gyrate with a radius smaller than the computational cells used near our dust sources (~10^4 km).

On the spatial scales used, the assumption of a cometary body being a dusty point source seems reasonable. However, in a more realistic situation dust particles may survive ion pickup long after ejection from their cometary parent. To analytically determine the shape and distribution of a cometary dust tail prior to mass loading the solar wind, we follow particles ejected from their cometary source, assuming they are subjected to only two basic forces: radiation pressure and solar gravitation. The ratio of these forces, β, is determined by particle size/mass and indicates whether ejected particles will have elliptic or hyperbolic trajectories with respect to the Sun.

Using the orbit of Comet C/2011 W3, but restricted to the ecliptic (xy) plane, we eject dust particles with bulk density $\rho_{\text{bulk}} = 0.4$ g cm^{-3} and diameters ranging from $d = 0.1$ μm to $d = 100$ μm starting at perihelion. At various times t_C, following perihelion ($t_C = 0$) we determine how the ejected particles are distributed. We will specifically look at $t_C = 6$, 12, 18, and 24 h after perihelion. Figure 1 shows a dust tail example for $t_C = 12$ h. All particles of the same β form curves called syndynes, while particles ejected at the same time form synchrone curves [*Mendis et al.*, 1985]. Like with the mass distribution, the smaller particles account for most of the dust tail volume.

Using spatial distribution data (e.g., Figure 1) to define tail-shaped mass-loading regions for our four snapshots, we run the SC component with a spread of particles more realistic than with a point source. This is done by taking the syndyne-/synchrone-generated particle distributions and reading them into the SC component model described above. Following the point source model by *Rasca et al.* [2014], a particle size distribution d^{-k} (with $k = 3.5$) is used in determining the overall mass distribution within the tail region and, as a result, our mass-loading source. For our first case, we keep the overall mass loss rate the same as with the point source simulations, with particles now spread out across our tail region, and determine the mass loss rate using a model by *Sekanina and Chodas* [2012]. For a second case, we increase the mass loss rate by a factor of 10. The exaggerated rate case considers a larger mass-loading cometary source, such as the much larger Comet C/2011 W3 [*Knight and Walsh*, 2013]. We assume dust is lost to the solar wind at a constant rate during the first 2 days following perihelion, giving a steady mass loss rate of 1.7×10^4 kg/s (1.7×10^5 kg/s for our exaggerated case). The result is the same mass-loading rate as the point source results, but spread across our new mass-loading region.

Equations (1)–(5) are solved on a spherical grid with extra levels of refinement around the cometary source for each t_C. Figure 2 shows radial velocity steady state solutions for the two different mass-loading rates. In both cases, solutions for each t_C are plotted together in the same panel. When the dust tail mass is more spread out, only a slight change in radial velocity is observed. However, results using our exaggerated mass-loading rate closely mimics point source results from *Rasca et al.* [2014], indicating that a tenth of the mass remains close to the source, while the remainder is too spread out to cause visible changes in the solar wind velocity. Figure 3 shows the separated densities ρ_{H} and ρ_{d_i} for $t_C = 18$ h from Figure 2 (right), indicating

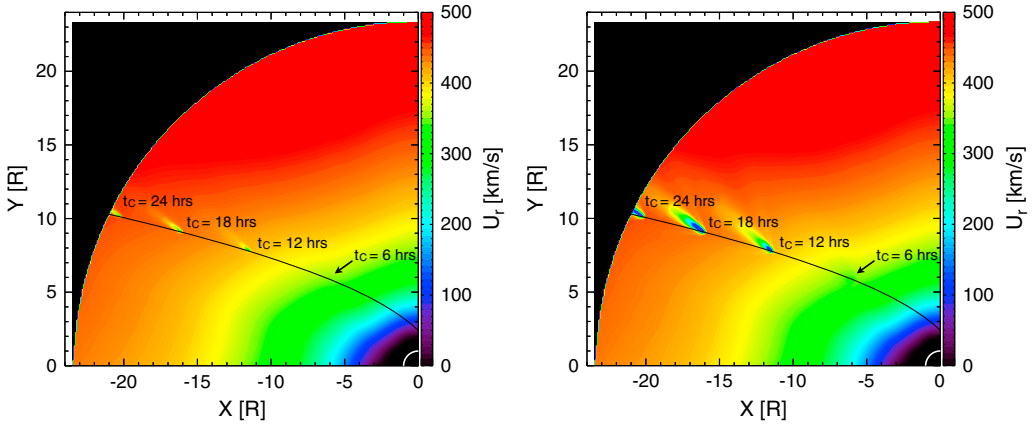

Figure 2. Radial velocity results from using a modified SC component to place a dust tail source along a sungrazing cometary trajectory (black curve) in the *xy* plane, using mass loss rates of (left) 1.7×10^4 kg/s and (right) 1.7×10^5 kg/s. Each t_C mass-loading result corresponds with tail-generated mass-loading regions similar to Figure 1.

where each species dominates in the mass loaded solar wind. The dust species primarily dominates in the immediate vicinity of the cometary source extending downstream approximately 1.5 $R_\odot$.

3. Solar Probe View

The upcoming Solar Probe Plus (SPP) mission will be taking direct observations of the solar corona within the next decade, launching in 2018 for a 7 year mission, making several passes through the solar corona. SPP's closest approach will be 8.5 $R_\odot$ from the solar surface [*Solar Probe Plus*, 2008]. We now look at how measurable solar wind parameters may appear when traveling downstream of a sungrazing comet such as Comet C/2011 W3. Several of SPP's orbits will also have approaches between 15 $R_\odot$ and 20 $R_\odot$ from the Sun, allowing use of our t_C = 18 h mass-loading results from Figure 2 (right).

We set up four possible SPP paths downstream of our t_C = 18 h mass-loading tail source (exaggerated) to show how changes in the solar wind will appear to the probe with changing distance from a cometary source. These paths have orbital characteristics similar to actual planned SPP passes near the Sun and are spread out evenly, from the cometary source to a few $R_\odot$ downstream. We can then determine how solar wind parameters such as velocity, plasma density, and magnetic field strength change as the probe travels along these paths.

Figure 4 shows the solar wind radial velocity, plasma density, and magnetic field strength in the vicinity of our mass-loading source with the four SPP orbits (1–4) drawn. Figure 4 also shows the changes in the solar

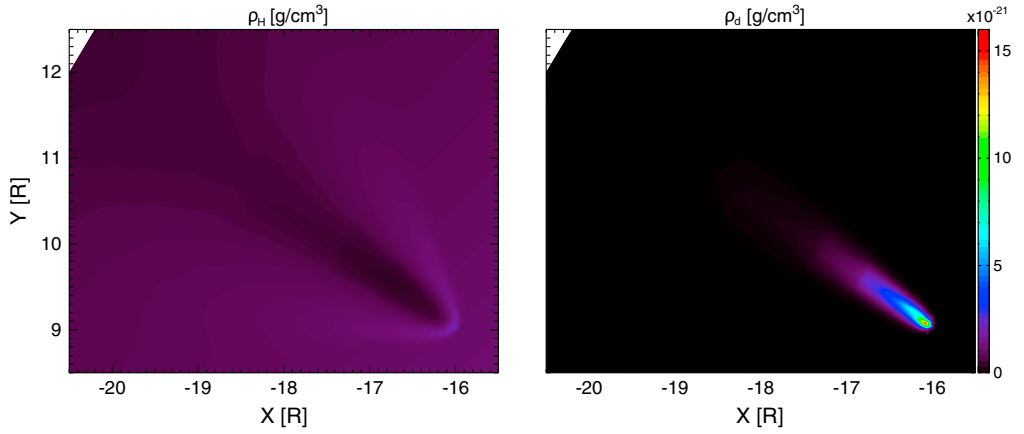

Figure 3. Mass densities ρ_H and ρ_{d_i} for hydrogen and ionized dust, respectively, in the vicinity of the t_C = 18 h mass-loading source from Figure 2 (right).

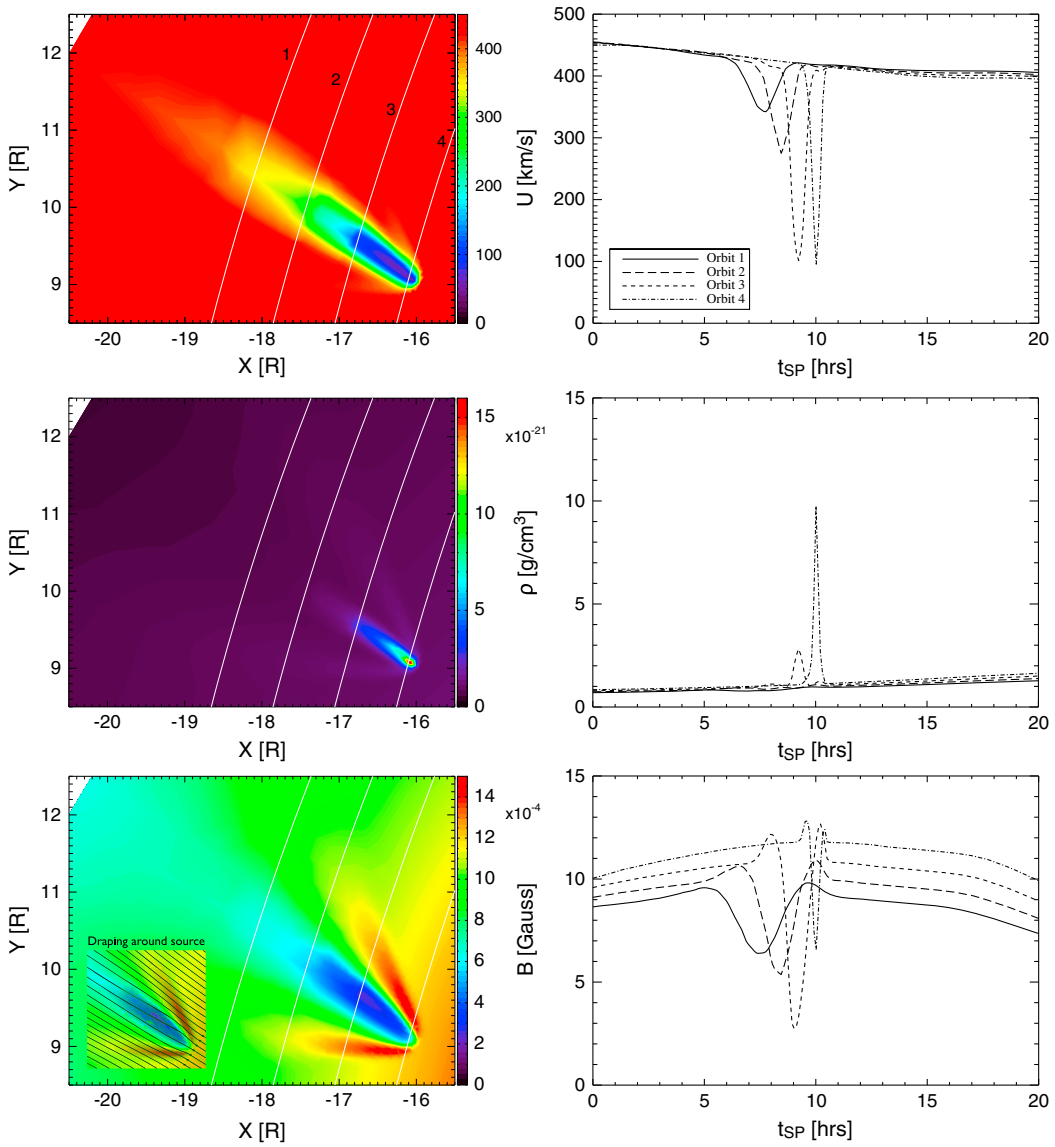

Figure 4. (top to bottom) Radial velocity, total density, and magnetic field strength profiles (right) along four probe paths (left), similar to planned Solar Probe Plus approaches through the solar corona.

wind that SPP would see along each orbit. The radial velocity and plasma density profiles show typical drops and spikes, respectively, associated with mass-loaded compressible flows, which decrease in magnitude downstream. The magnetic field strength profiles show more interesting results, revealing that signatures in the magnetic field indicating a mass-loading dust source will occur before any observable changes in wind velocity or plasma density. Large drops in the magnetic field strength directly downstream will be preceded/proceeded by jumps in the field strength, in agreement with magnetic draping around mass-loading regions and resulting downstream magnetic cavities [*Rasca*, 2013] and with interplanetary magnetic field enhancements observed by the ISEE-3 spacecraft when encountering a comet [*Russell*, 1990]. Variations in mass-loading rates would alter the strengths in any observed drops/peaks.

This is of course a simplified view of a cometary orbit around the Sun, with the comet and SPP orbiting in the same plane. Cometary orbits are often tilted significantly with respect to the ecliptic plane, making an SPP encounter with a cometary tail less likely than in our simplified case. However, the Solar and Heliospheric Observatory (SOHO) and Solar Terrestrial Relations Observatory (STEREO) spacecraft have discovered thousands of sungrazing comets over the past decade, revealing a high frequency of previously unknown visitors to the solar corona. The majority of these comets belong to a family called the Kreutz sungrazers, which

originated from a single parent comet that broke apart several centuries ago. The vast majority of sungrazers discovered by SOHO and STEREO are from the Kreutz group, with nearly 1600 discovered from 2004 to 2013 [*Sekanina and Kracht*, 2013]. On average, one Kreutz sungrazer reached perihelion every 2 days during that time period.

Since Kreutz sungrazers all share similar orbital elements and account for most of the known sungrazing comets, it is rather straightforward to determine the general likelihood of SPP encountering a Kreutz sungrazing comet. Assuming typical Kreutz orbital elements (140° inclination, 250–280° longitude of perihelion, 1–2 $R_\odot$ perihelion distance, ~700 year orbital period), several of SPP's planned inner orbits through the corona pass 5–10 $R_\odot$ directly downstream of the descending node of the Kreutz orbits, depending on the specific perihelion longitude and distance, close enough to detect dust or possible variations in the solar wind. Considering the velocity and dust coverage (e.g., Figure 1), the dust tail will only intersect SPP's path for approximately 3 h every 2 days (on average), giving SPP a 6% chance of encountering a Kreutz cometary dust tail during each of its closest approaches to the Sun. However, a large group of bright Kreutz sungrazers is predicted to arrive within the next decade, with Comet C/2011 W3 possibly being the first Great Comet of this forthcoming group [*Sekanina and Chodas*, 2007; *Sekanina and Kracht*, 2013], which would help increase the likelihood of SPP encountering a sungrazing comet.

4. Discussion and Conclusions

When using the tail source model, much of the ejected mass is still near the cometary source, generating a similar imprint on the solar wind velocity as with a point source. However, with the mass spread out, the drop in the solar wind speed is significantly lower. An order of magnitude increase of the mass-loading source is enough to account for the dispersion of mass and regain comparable results to the point source model. Additionally, the arcing nature of the dust tail is not reflected in any of our results shown. From additional simulations for the tail source cases, the source term would need to be increased by a factor of 10^3 for any arcing features to become evident in the radial velocity, but this rate will severely disrupt the coronal plasma near the cometary source.

With the prospects of future in situ coronal data, we looked at signatures in the solar wind indicating how an upstream cometary source would appear to a passing space probe. The results show a general drop in radial velocity and increase in plasma density, both decreasing in magnitude with distance from the cometary source. Magnetic field strength profiles along a space probe orbit reveal a magnetic cavity directly downstream, flanked by jumps in field strength due to magnetic draping. These results will hopefully establish the basic framework to compare future in situ observations with theoretical modeling of mass-loading due to dust.

Acknowledgments

The data for this paper are available at the University of Colorado at Boulder's Institute for Modeling Plasma, Atmospheres and Cosmic Dust. Additionally, we would like to thank B. van der Holst, T. Gombosi, and G. Tóth of the University of Michigan's Center for Space Environment Modeling for providing help with SC component of the SWMF.

The Editor thanks David McComas and an anonymous reviewer for their assistance in evaluating this paper.

References

Biermann, L., B. Brosowski, and H. U. Schmidt (1967), The interaction of the solar wind with a comet, *Sol. Phys.*, *1*, 254–284.

Hollweg, J. V. (1986), Transition region, corona, and solar wind in coronal holes, *J. Geophys. Res.*, *91*, 4111–4125.

Knight, M. M., and K. J. Walsh (2013), Will Comet ISON (C/2012 S1) survive perihelion?, *Astrophys. J. Lett.*, *776*, L5.

Mann, I., and R. H. MacQueen (1996), Observation and analysis of the F-corona brightness, *Adv. Space Res.*, *17*, 353–356.

Mendis, D. A., H. L. F. Houpis, and M. L. Marconi (1985), The physics of comets, *Fund. Cosmic Phys.*, *10*, 1–380.

Rasca, A. P. (2013), Modeling solar wind mass-loading due to dust in the solar corona, PhD thesis, Univ. of Colorado at Boulder, Boulder, Colo.

Rasca, A. P., and M. Horányi (2013), Solar wind mass-loading due to dust, *AIP Conf. Proc.*, *1539*, 418–421.

Rasca, A. P., M. Horányi, R. Oran, and B. van der Holst (2014), Modeling solar wind mass-loading in the vicinity of the Sun using 3-D MHD simulations, *J. Geophys. Res. Space Physics*, *119*, 18–25, doi:10.1002/2013JA019365.

Russell, C. T. (1990), Interplanetary magnetic field enhancements: Evidence for solar wind dust trail interactions, *Adv. Space Res.*, *36*, 159–162.

Russell, C. T., L. K. Jian, and J. G. Luhmann (2009), An unusual current sheet in an ICME: Possible association with C/2006 P1 (McNaught), *Geophys. Res. Lett.*, *36*, L07105, doi:10.1029/2009GL037615.

Sekanina, Z., and P. W. Chodas (2007), Fragmentation hierarchy of bright sungrazing comets and the birth and orbital evolution of the Kreutz system. II. The case for cascading fragmentation, *Astrophys. J.*, *663*, 657–676.

Sekanina, Z., and P. W. Chodas (2012), Comet C/2011 W3 (Lovejoy): Orbit determination, outbursts, disintegration of nucleus, dust-tail morphology, and relationship to new cluster of bright sungrazers, *Astrophys. J.*, *757*, 127.

Sekanina, Z., and R. Kracht (2013), Population of SOHO/STEREO Kreutz sungrazers and the arrival of comet C/2011 W3 (Lovejoy), *Astrophys. J.*, *778*, 24.

Solar Probe Plus (2008), Report of the science and technology definition team, *Technical Report*, Goddard Space Flight Center, NASA, Greenbelt, Md.

Tóth, G., et al. (2012), Adaptive numerical algorithms in space weather modeling, *J. Comp. Phys.*, *231*, 870–903.

van der Holst, B., W. B. Manchester, R. A. Frazin, A. M. Vásquez, G. Tóth, and T. I. Gombosi (2010), A data-driven, two-temperature solar wind model with Alfvén waves, *Astrophys. J.*, *725*, 1373–1383.